RSC Advances

ROYAL SOCIETY OF CHEMISTRY

PAPER

View Article Online
View Journal | View Issue

Cite this: *RSC Adv.*, 2026, **16**, 25596

Waste-derived-lignin based hydrogel as a reusable adsorbent for efficient removal of dyes from aqueous solution

Umme Toufika Jannat,[a] Md. Anamul Haque, *[a] Sharuk Alam Aumi,[a] Swapan Kumer Ray,[b] Mohammad Moniruzzaman,[b] Md. Sarwar Jahan,[b] Md. Aftab Ali Shaikh [a] and Md. Qamrul Ehsan[a]

Wastewater contamination by synthetic dyes poses a significant environmental challenge due to their persistence, toxicity, and resistance to degradation. In this study, a lignin based hydrogel was synthesized and appraised as an efficient and sustainable adsorbent for removal of crystal violet (CV) and rhodamine B (RhB) dyes from aqueous solution. Prior to synthesis, lignin was extracted from black liquor, a waste-by-product of pulp and paper processing, and incorporated in a poly(vinyl alcohol) (PVA) gel matrix *via* a one-pot crosslinking reaction with epichlorohydrin as the crosslinking agent. The resulting lignin/PVA hydrogel was characterized by using Fourier-transform infrared spectroscopy, thermogravimetric analysis, scanning electron microscopy coupled with energy-dispersive spectroscopy, and tensile testing, confirming a porous structure with abundant functional groups. Batch adsorption experiments were conducted by varying the initial dye concentration, contact time, pH, and adsorbent dosage. The lignin/PVA hydrogel showed removal efficiencies of 86 and 69% for CV and RhB dye, respectively, with maximum adsorption capacities of 250.9 mg g^{-1} for CV and 19.4 mg g^{-1} for RhB. Isotherm analysis justified that adsorption followed the Freundlich isotherm model, suggesting multilayer adsorption on a heterogeneous surface, while kinetic studies revealed a pseudo-second-order nature. Thermodynamic analysis confirmed that the adsorption process is spontaneous and endothermic. The adsorption mechanism is governed by a combination of electrostatic interactions, hydrogen bonding, and π–π interactions. The hydrogel also demonstrated worthy reusability, maintaining performance over five adsorption–desorption cycles. Therefore, the lignin/PVA hydrogel could be a cost-effective, sustainable, and reusable adsorbent for dye removal from wastewater.

Received 21st February 2026
Accepted 7th May 2026

DOI: 10.1039/d6ra01545j

rsc.li/rsc-advances

1. Introduction

Rapid industrialization has intensified significant environmental concerns, with water pollution emerging as a critical global concern.[1,2] Industrial effluents, agricultural runoff, and domestic wastewater significantly degrade water quality.[3,4] Among these, the discharge of synthetic dyes from textile, paper, leather, and cosmetic industries has become a major contributor to aquatic pollution.[5,6] These dyes are typically non-biodegradable, toxic, and resistant to degradation under light, heat, and microbial attack due to their stable aromatic structures.[7] Crystal violet (CV) and rhodamine B (RhB) are two commonly used synthetic dyes known for their mutagenic, carcinogenic, and toxic effects on human health and aquatic life.[8,9] CV, a triphenylmethane dye, interferes with cell division and has been reported to cause skin irritation and liver toxicity.[8] RhB, a xanthene dye, is suspected of neurotoxicity and reproductive toxicity and may cause long-term damage to the environment.[10,11] A range of treatment approaches has been developed to address dye contamination in wastewater, including membrane filtration, chemical oxidation, coagulation–flocculation, and biological degradation.[12–15] However, many of these approaches are either costly, produce secondary pollutants, or are inefficient in removing stable dye molecules.[16] Among these methods, adsorption has emerged as a promising approach owing to its simplicity, high efficiency, and low energy requirements.[17,18] In this context, attention has been shifted towards the evolution of numerous adsorbents either derived or synthesized from various sources.[19] Lignin, an abundant aromatic biopolymer has shown significant potential as an adsorbent due to its rich functional groups, such as hydroxyl and methoxy groups.[20,21] However, the development of waste-generated, low-cost, sustainable, and efficient lignin adsorbents remains a key challenge of research. In particular, lignin can be extracted from waste black liquor generated during pulp and paper processing, which represents the primary industrial source of lignin and a largely underutilized byproduct. The

[a]*Department of Chemistry, University of Dhaka, Dhaka-1000, Bangladesh. E-mail: anamul@du.ac.bd*

[b]*Bangladesh Council of Scientific and Industrial Research (BCSIR), Dhaka-1205, Bangladesh*

abundant availability, rich functional groups, and aromatic structure of lignin make it a promising candidate for value-added applications, including adsorption materials. Nevertheless, the direct utilization of lignin is often limited by its poor processability, dispersibility, and unavailable surface active sites towards its adsorption performance.[22] To overcome these limitations, embedding lignin into a polymer matrix can enhance its adsorption efficiency by improving its structural integrity and increasing the accessibility of active sites.[23] Recent studies have demonstrated the growing potential of lignin-based hydrogels in environmental remediation, particularly for dye and heavy metal removal, highlighting the importance of structural design and functional group interactions. Additionally, various studies on lignin-based composite hydrogels primarily focus mainly on enhancing adsorption performance through composite design, reaction pathway and kinetic/isotherm evaluation.[24,25] Therefore, the development of hydrogel adsorbents based on waste-derived lignin has emerged as a key research direction for the sustainable valorization of industrial byproducts and efficient wastewater treatment. On the other hand, polyvinyl alcohol (PVA) is a widely used polymer matrix for hydrogel preparation due to its hydrophilicity, biocompatibility, and abundant hydroxyl groups. Therefore, the combination of lignin derived from waste-black-liquor with PVA through appropriate crosslinking strategies provides a promising route to develop sustainable hydrogel adsorbents with enhanced structural stability and adsorption performance.[26]

In this study, a lignin/PVA hydrogel has been synthesized utilizing waste-derived lignin and evaluated for the removal of crystal violet (CV) and rhodamine B (RhB) from aqueous solutions. Lignin was extracted from waste-black-liquor produced during industrial pulp and paper processing. The extracted lignin and the synthesized lignin/PVA hydrogel were characterized using Fourier Transform Infrared Spectroscopy (FT-IR), Scanning Electron Microscopy with Energy Dispersive X-ray Spectroscopy (SEM-EDS), and Thermogravimetric Analysis (TGA) to determine its structural, morphological, and thermal properties. Mechanical testing was also performed to assess the hydrogel's strength and elasticity. Batch adsorption experiments were systematically carried out to investigate the effect of initial dye concentration, contact time, pH, and adsorbent dosage. In addition, adsorption isotherms and kinetics models were applied to elucidate the adsorption behavior and underlying mechanism. The results suggest that the adsorption process is governed by a combination of hydrogen bonding, electrostatic interactions, and π–π interactions, highlighting the effectiveness of the lignin/PVA hydrogel as a sustainable and efficient adsorbent for dye-contaminated wastewater treatment. Furthermore, the hydrogel demonstrated satisfactory regeneration and reusability, retaining a substantial portion of its adsorption capacity over five cycles, indicating its potential as a sustainable and cost-effective adsorbent for industrial wastewater treatment.

2. Materials and method

2.1 Materials

Poly(vinyl alcohol) (99% hydrolyzed, CAS no: 9002-89-5), epichlorohydrin (99.52 g mol^{-1}, CAS no: 106-89-8), crystal violet (407.98 g mol^{-1}, CAS no: 548-62-90), rhodamine B (479.01 g mol^{-1}, CAS no: 81-88-9) were purchased from Sigma-Aldrich. Hydrochloric acid (HCl) and sodium hydroxide (NaOH) were obtained from Merck (India).

2.2 Extraction of lignin

Lignin was isolated from black liquor (by-product) obtained through kraft pulping of eucalyptus wood. 2 M sulfuric acid was added to the collected black liquor to adjust the pH at 2.[27] This pH adjustment caused the color of the black liquor to change from black to brown, leading to the formation of a precipitate. The mixture was left undisturbed overnight to allow for complete settling. The precipitate was then washed with DI water until the pH of the mixture reached 5 to 6.[28] The lignin precipitate was collected by centrifugation and subsequently dried in an oven at 50 °C.

2.3 Synthesis of lignin/PVA hydrogel

The lignin/PVA hydrogels were synthesized using a one-pot reaction with epichlorohydrin (ECH) as a crosslinking agent (Scheme 1).[29] In brief, 0.8 g PVA was dissolved in 5.0 mL 1.0 M NaOH solution under heating at 80 °C and continuous stirring (~400 rpm) in an oil bath for 1 h using a magnetic stirrer (model: MS-H380-Pro DLAB). Once fully dissolved, lignin was gradually added to the PVA solution and stirred until a homogeneous mixture was achieved. 0.4 mL ECH was then added to the mixture, and the solution was placed in a heating oven for 2 h to complete the hydrogel formation process. Five different hydrogels were prepared by varying the amount (0.10 to 0.45 g) of lignin. The amount of ECH was preserved constant for all compositions of lignin/PVA hydrogel to sustain a consistent crosslinking within PVA matrix. Lignin content was only varied to investigate it effects on the structural properties and adsorption performances of the lignin/PVA hydrogel. The compositions of the lignin/PVA hydrogel were also summarized in Table S1. After synthesis, the hydrogels were immersed in DI water for 24 h. The DI water was then replaced 7 times with an interval of 24 h to diffuse out any excess lignin, ECH, PVA, and residual NaOH.

2.4 Characterization of lignin, PVA gel and lignin/PVA hydrogel

2.4.1 Physical and chemical characterization. Swelling ratio is a key parameter used to characterize hydrogel which provides information about the ability of a hydrogel to absorb and retain water or other solvent.[30] For swelling ratio measurement (weighing ratio), immediately after synthesis, the hydrogels were wiped with filter paper and weighed to obtain the initial mass (W_0). Then, the hydrogel was immerged in DI water until equilibrium swelling was reached. The water swollen hydrogel was wiped again with filter paper and weighed to obtain the equilibrium swollen mass (W_e). Swelling ratio (W_e/W_0) of the hydrogels were then achieved. The dry mass of the equilibrium swollen hydrogel was estimated by using a moisture analyzer [Shimadzu, Model MOC63u]. About 2 g of water swollen hydrogel was placed on the pan of moisture balance

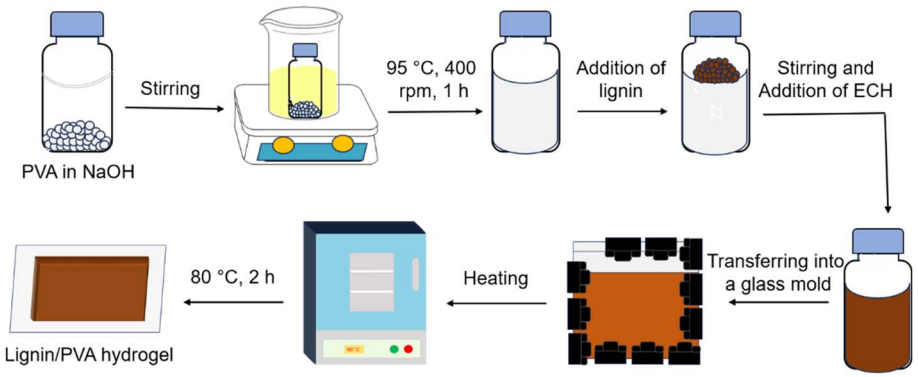

Scheme 1 Synthesis of lignin/PVA hydrogel.

and heated at 120 °C until a constant dry mass (W_{dry}) of hydrogel was obtained. The equilibrium swollen hydrogel was employed for the entire adsorption study while dry mass of hydrogel was considered only for adsorption capacity calculations.

To identify the characteristic functional groups, FT-IR spectra of the extracted lignin, PVA hydrogel, and lignin/PVA hydrogel were obtained using an FT-IR spectrometer (Model: Frontier, PerkinElmer). The spectra were recorded over the frequency range of 4000–650 cm^{-1}. Surface morphologies and elemental compositions of the extracted lignin, PVA gel, and lignin/PVA gel were investigated using scanning electron microscopy (SEM) with energy dispersive spectroscopy (EDS) (Model: ZEISS EVO 18, Carl Zeiss, Germany). For each sample, three SEM images were captured at different magnifications ranging from 5 K to 25 K using an applied high voltage of 15 kV. The EDS analysis was conducted to determine the elemental composition of the samples.

Brunauer–Emmett–Teller (BET) surface area analysis was conducted to evaluate the surface characteristics of the extracted lignin. Prior to analysis, the lignin sample was dried at 105 °C for several hours to remove residual moisture. The dried sample was then placed in a sample tube and degassed under a continuous flow of nitrogen gas at 110 °C for 8 h to eliminate physically adsorbed gases and surface impurities. Nitrogen adsorption–desorption measurements were carried out using a surface area analyzer (BET Microtrac BELSORP Max-II). The sample was cooled to 77 K using liquid N_2 during the analysis. N_2 was introduced incrementally, and the adsorption isotherm was recorded by measuring the volume of gas adsorbed as a function of relative pressure (P/P_0). The specific surface area was calculated using the BET method within the relative pressure range of $P/P_0 = 0.05$–0.30, which corresponds to the standard linear region of the BET plot.

2.4.2 Thermal characterization. Thermal properties of the extracted lignin and the synthesized hydrogels were examined using a thermogravimetric analyzer (Model: Pyris 1 TGA, PerkinElmer). A specified quantity of each oven dried sample was placed in the instrument with a heating rate 10 °C min^{-1}, which continuously measured the mass loss as the temperature increased to 700 °C. This technique was used to obtain thermogravimetric (TGA) curves and differential thermogravimetric (DTG) curves.

2.4.3 Mechanical characterization. The mechanical properties of the synthesized hydrogels were evaluated through tensile testing using a universal testing machine (model: ZL-8001A). Measurements were performed on samples with a gauge length of 36 mm, width of 4.5 mm, and thickness of 1.4 mm, using the hydrogels in their as-prepared condition. The tensile tests were conducted at a crosshead speed of 100 mm min^{-1} under a maximum load capacity of 100 N. During the tests, stress–strain curves were recorded, from which key mechanical parameters including tensile strength, elongation at break, and toughness were derived. Tensile strength was determined as the maximum stress sustained before failure, while elongation at break was calculated as the strain corresponding to the fracture point. Toughness, representing the energy absorbed by the material prior to rupture, was obtained by calculating the area under the stress–strain curve. Data analysis, including curve fitting and area integration, was carried out using OriginPro software.

2.4.4 Adsorption study. The adsorption performance of the lignin/PVA hydrogel was evaluated for the removal of dyes, crystal violet (CV) and rhodamine B (RhB), through batch adsorption experiments.[31] For CV dye adsorption, batch experiments were conducted by immersing a fixed amount of lignin/PVA hydrogel in 20 mL of aqueous dye solutions. The initial dye concentrations ranged from 2.0×10^{-5} to 12.0×10^{-5} M. The hydrogel dosage was varied between 1.0 and 5.0 g to study the effect of adsorbent amount on dye removal efficiency. Additionally, the impact of solution pH on adsorption performance was investigated across a pH range of 2 to 9. Similarly, batch adsorption experiments were performed for RhB dye using 20 mL of dye solutions with initial concentrations ranging from 1.0×10^{-6} to 14.0×10^{-6} M. The hydrogel dosage was varied between 1.0 g and 8.0 g. The influence of pH was also assessed within the range of pH 2 to 9. It is worth to mention here that the total system volume (adsorbent hydrogel + dye solution) was maintained constant at 20 mL to minimize the volume effect associated with varying adsorbent dosage. The dye concentration was adjusted accordingly by preparing the solution from a higher-concentration stock, ensuring that the final

concentration corresponded to the desired initial concentration, calculated based on the total system volume of 20 mL. The initial (before adsorption) and final concentrations (after adsorption) of dye were determined using a UV-visible spectrophotometer (ASC-7000, Shimadzu, Japan) at characteristic wavelengths of 581.5 nm for CV and 553.5 nm for RhB. Optimal adsorption conditions for these dyes, including concentration, adsorbent dosage, pH, and contact time, were identified based on the highest percent removal observed. The corresponding removal efficiency (RE) and adsorption capacity (q) of the lignin/PVA hydrogel were calculated by using these equations:

$$\mathrm{RE_e}\ (\%) = \frac{C_0 - C_e}{C_0} \times 100 \quad (1)$$

$$q_e = \frac{C_0 - C_e}{W_{dry}} \times V \quad (2)$$

$$\mathrm{RE}_t\ (\%) = \frac{C_0 - C_t}{C_0} \times 100 \quad (3)$$

$$q_t = \frac{C_0 - C_t}{W_{dry}} \times V \quad (4)$$

where C_0, C_t, and C_e represent the initial concentration, the concentration at time t, and the equilibrium concentration, respectively. $\mathrm{RE_e}$ (%) and RE_t (%) denote the removal efficiency at equilibrium and at time t, respectively. q_e and q_t are the adsorption capacities (mg g^{-1}) at equilibrium and at time t, respectively. W_{dry} refers to the dry mass of the adsorbent in gram, and V (L) indicates the volume of the adsorbate solution.[32] All adsorption experiments were performed in triplicate, and the average values are reported. The associated error bars in the figures represent the standard deviation of the measurements.

For thermodynamic study, adsorption experiments were also conducted at different temperatures (298, 308, 318, and 328 K) under optimized conditions of initial dye concentration, pH, contact time, and adsorbent dosage. A fixed amount of equilibrium swollen hydrogel was added to 20 mL of dye solution with a known initial concentration. The mixtures were maintained under static conditions in a thermostatic water bath to ensure constant temperature throughout the experiment. After reaching adsorption equilibrium (96 h), the residual dye concentration (C_e) was determined using a UV-vis spectrophotometer. The equilibrium adsorption capacity (q_e) was calculated accordingly.

To evaluate the effect of enhanced mass transfer on adsorption performance, batch adsorption experiments were conducted under stirring conditions. 1.0 g of lignin/PVA hydrogel was added to 20 mL of dye solution (CV or RhB). The mixture was agitated using a horizontal shaker at a reciprocating shaking (range: 40 mm, speed: 50 turns per min) at 298 K. At specific time intervals, aliquots of the solution were withdrawn, and the residual dye concentration was determined using a UV-visible spectrophotometer at the characteristic wavelength of each dye.

3. Results and discussion

Lignin powder (extracted from waste-black-liquor), poly(vinyl alcohol) gel (PVA gel) and lignin/PVA hydrogel are shown in Fig. 1. Mechanically stable lignin/PVA hydrogel was successfully obtained in presence of ECH crosslinker. It is to mention here that stable hydrogel was not formed in the absence of ECH confirming that ECH is essential for establishing covalent crosslinking and structural integrity of the lignin/PVA hydrogel. ECH acts as a bi-functional crosslinking agent that reacts with hydroxyl (–OH) groups of both PVA and lignin under alkaline conditions, leading to the formation of a three-dimensional network structure. Under alkaline conditions, –OH groups of PVA and lignin are partially deprotonated to form alkoxide ions ($–O^-$), which are more nucleophilic. The alkoxide groups attack the epoxide ring of ECH, resulting in ring opening and formation of β-hydroxy ether intermediates. The remaining chloromethyl group ($–CH_2Cl$) in ECH further reacts with another hydroxyl group, forming ether linkages ($–O–CH_2–CHOH–CH_2–O–$) and connecting polymer chains. Although ECH is a toxic compound, it is consumed during the crosslinking reaction and the resulting hydrogels are thoroughly washed to remove residual reagents, leaving minimum potential environmental risks. Although ECH was used as an effective crosslinking agent in this study, environmentally friendly alternatives such as citric acid and other polycarboxylic acids could be explored as alternative crosslinkers.

3.1 Structure, morphology and property evaluation

3.1.1 Swelling ratio. Swelling ratios of the synthesized hydrogels as a function of varying lignin concentrations are

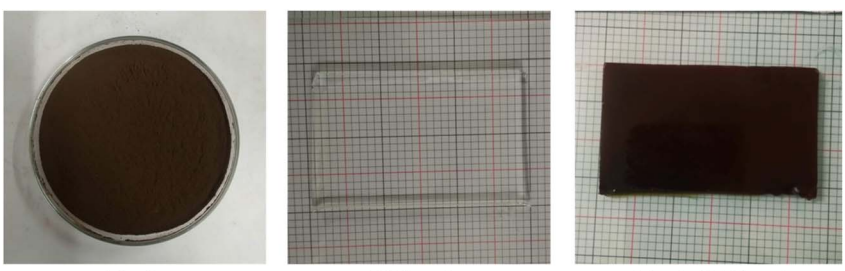

Fig. 1 Photographs of extracted lignin (powder), PVA gel and lignin/PVA hydrogel.

Table 1 Swelling ratio of the lignin/PVA hydrogels at various lignin concentrations

Lignin (%)	Weight as-prepared, W_0 (g)	Weight at equilibrium swelling, W_e (g)	Dry weight, W_{dry} (g)	Swelling ratio (W_e/W_0)
0	1.915	5.785	0.1532	3.02
1.0	0.863	4.865	0.0777	5.65
2.0	0.463	3.531	0.0463	7.63
3.0	0.687	6.927	0.0755	10.07
4.0	0.798	8.518	0.0958	10.67
4.5	0.719	7.712	0.0899	10.72

summarized in Table 1. As shown in Table 1 and Fig. S1, the swelling ratio initially increases sharply with the addition of lignin, followed by a more gradual rise at higher lignin contents. This trend suggests that the incorporation of lignin enhances the hydrogel's water-retention capacity, likely due to the presence of hydrophilic functional groups, such as phenolic hydroxyl groups, within the lignin structure.[33] However, beyond a certain concentration, the swelling ratio of the hydrogels remains relatively constant. This plateau effect is due to the saturation of the PVA hydrogel matrix with lignin molecules, suggesting that further addition of lignin to the reaction mixture no longer significantly affects its incorporation into the hydrogel matrix.[34]

3.1.2 FT-IR. FT-IR analysis was performed for the extracted lignin, PVA gel, and lignin/PVA hydrogel to confirm the presence of functional groups and structural characteristics. Fig. 2 presents the FT-IR spectra with distinct functional group peaks for each sample. The broad peak observed at 3285 cm^{-1} for lignin, lignin/PVA hydrogel and PVA gel spectra attributed to –OH stretching. The presence of peaks centered at 2910 cm^{-1}, 1420 cm^{-1}, 1328 cm^{-1}, and 1085 cm^{-1} associated with C–H stretching, –OH bending, C–H bending, and C–O–C stretching, respectively. The spectrum of lignin displays prominent bands at 1609 and 1513 cm^{-1}, attributed to aromatic C=C stretching vibrations from the aromatic rings.[28] In the PVA hydrogel, two weak peaks appear at 1655 and 1740 cm^{-1}, associated with C=C and C=O stretching vibrations, respectively. The C=O peak likely originates from residual acetate groups that remain after partial hydrolysis or oxidation during PVA synthesis.[35] In the lignin/PVA hydrogel, both lignin and PVA characteristic peaks in the region 2100–1500 cm^{-1} are evident, signifying the successful incorporation of lignin into the hydrogel matrix. The interaction between lignin and PVA is accompanied by the combination of hydrogen bonding and ECH covalent cross-linking between –OH groups of PVA and phenolic/aliphatic –OH groups of lignin. In addition to the qualitative FT-IR analysis, peak shift further supports the presence of hydrogen bonding interactions. A noticeable red shift of the –OH stretching vibration from ~3285 cm^{-1} in pure PVA hydrogel to ~3260–3270 cm^{-1} in the lignin/PVA hydrogel ($\Delta \approx$ 15–25 cm^{-1}), along with peak broadening, indicates the formation of intermolecular hydrogen bonding between hydroxyl groups of PVA and lignin. Minor shifts in the C–O stretching region further support the involvement of hydroxyl groups in these interactions.

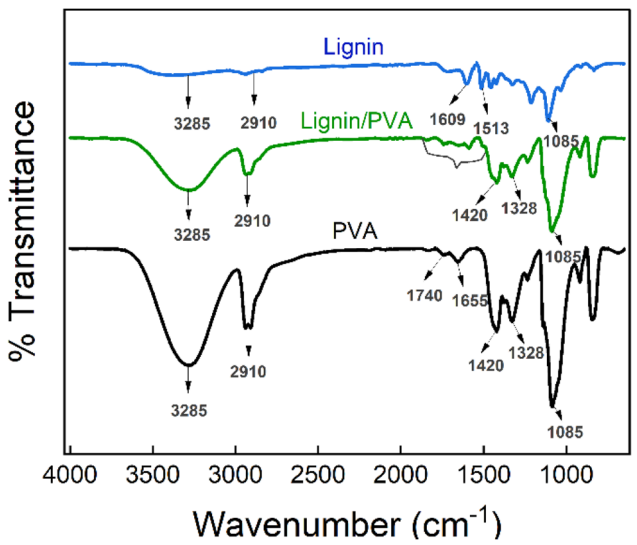

Fig. 2 FT-IR spectra of extracted lignin, lignin/PVA hydrogel and PVA gel.

3.1.3 SEM-EDS. SEM micrographs (Fig. 3) show the surface morphology of extracted lignin (Fig. 3a), lignin/PVA (Fig. 3b), and PVA gel (Fig. 3c). The images reveal that the extracted lignin exhibits a granular form with irregularly sized grains and a rough, compact surface. The PVA hydrogel, in contrast, shows a smooth and compact structure. Upon incorporation of lignin into the PVA gel, the resulting lignin/PVA hydrogel displays a rough and porous surface. This porous architecture is likely to enhance the hydrogel's specific surface area, increasing its capacity for dye and heavy metal ion adsorption.[36] To assess the elemental composition of each material, EDS was performed and analyzed which are as shown in Fig. S2. Although, EDS data confirms that all samples are primarily composed of C and O, the relative elemental compositions do not show significant differences due to the similar elemental compositions of lignin and PVA. However, EDS elemental composition shows intermediate values between lignin and PVA, which supports the coexistence of both components and therefore incorporation of lignin into the PVA matrix in agreements with FT-IR and SEM.[37]

3.1.4 BET analysis. The nitrogen adsorption–desorption isotherm of lignin is shown in Fig. 4a. The specific surface area obtained using the BET method within the relative pressure

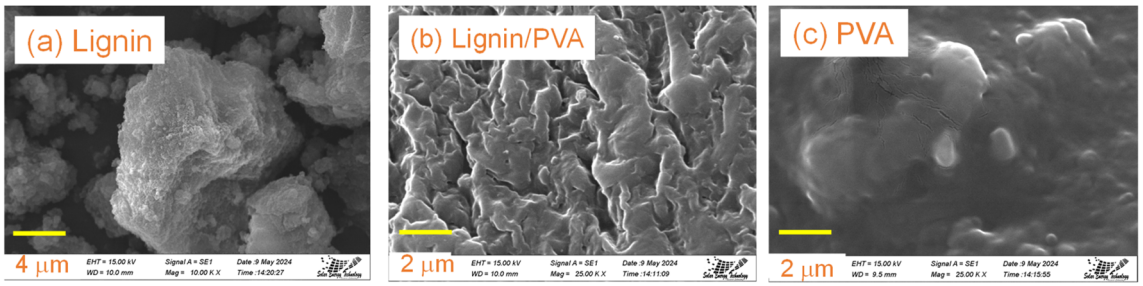

Fig. 3 SEM images of (a) extracted lignin, (b) lignin/PVA hydrogel, and (c) PVA gel.

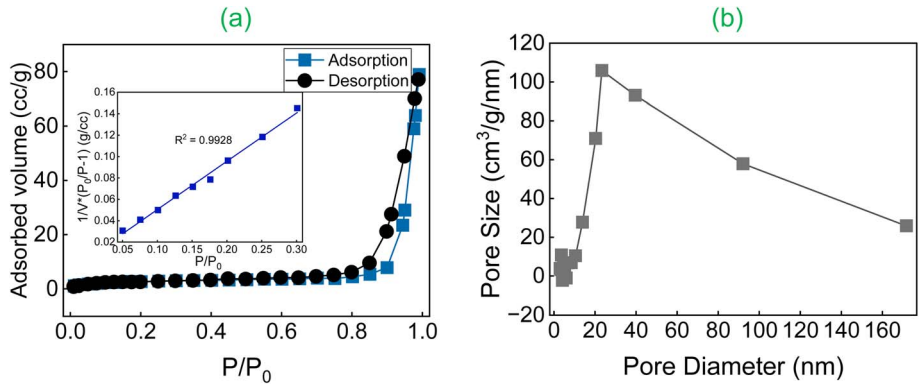

Fig. 4 (a) Brunauer–Emmett–Teller (BET) N_2 adsorption/desorption isotherm of extracted lignin showing type IV behavior with a hysteresis loop at higher relative pressures and (b) pore size distribution of lignin.

range of $P/P_0 = 0.05$–0.30, which corresponds to the standard linear region of the BET plot (Fig. 4a, inset) revealed a relatively low surface area of 9.6 $m^2\ g^{-1}$, which is characteristic of its dense and poorly developed porous structure. The total pore volume was determined as 0.1198 $cm^3\ g^{-1}$ at a relative pressure close to unity. The average pore diameter was calculated from BJH distributions as 24.94 nm (Fig. 4b), further supporting mesoporosity. The adsorption–desorption isotherm exhibited a hysteresis loop at higher relative pressures, suggesting capillary condensation within the mesoporous and corresponding to a typical type-IV isotherm behavior. Despite the mesoporous nature, the low surface area implies a limited number of accessible adsorption sites, which can be attributed to the compact and irregular arrangement of lignin macromolecules. This highlights the importance of incorporating lignin into a hydrogel matrix, where the three-dimensional network can improve the accessibility of functional groups (in agreement with the SEM image, Fig. 3b) and enhance adsorption performance. It should be noted that BET analysis of the hydrogel was not performed, as drying may lead to structural collapse and does not accurately represent the hydrated state during adsorption.

3.1.5 TGA. Thermal stability and decomposition behavior of lignin, PVA gel, and lignin/PVA hydrogel were examined by TGA/DTG and the thermograph are shown in Fig. 5. An initial weight loss in lignin from 40 °C to 130 °C occurs due to the evaporation of water [Fig. 5a]. With further increase in temperature, significant decrease of weight was noticed between 150 °C and 500 °C corresponding to the breakdown of low-molecular-weight phenols, such as guaiacol, and side-chain degradation. This broad decomposition ranges between 150 °C and 500 °C is the clear indication of its complex molecular structure and various functional groups. Predominant loss of weight between 500 °C and 650 °C was occurred due to the aromatic ring decomposition. Approximately 14% of the lignin content remained as biochar and ash residue at the end, indicating high thermal stability.[38] On the other hand, PVA gel [Fig. 5b] shows a five-step thermal decomposition pattern. The first decomposition, occurring below 220 °C, reflects the loss of moisture and dehydration, which may involve cyclization reactions among hydroxyl groups. The subsequent decomposition steps, beginning around 250 °C, corresponds to the breakdown of the polymer backbone with rapid degradation rate in the range 330–420 °C, leaving no residual mass above 620 °C.[39] It is found that lignin/PVA hydrogel (Fig. 5c) demonstrates thermal behavior similar to PVA hydrogel up to 500 °C. Above 500 °C, aromatic ring of incorporated lignin begins to break down with a rapid degradation rate. However, the overall thermal stability of the lignin/PVA hydrogel exceeds that of PVA gel, attributes to the reinforcing effect of lignin within the hydrogel matrix.[40]

3.1.6 Mechanical behavior of lignin/PVA hydrogel. The mechanical behavior of the lignin/PVA hydrogels was evaluated through tensile testing, and the resulting stress–strain curves are presented in Fig. 5d with key parameters summarized in

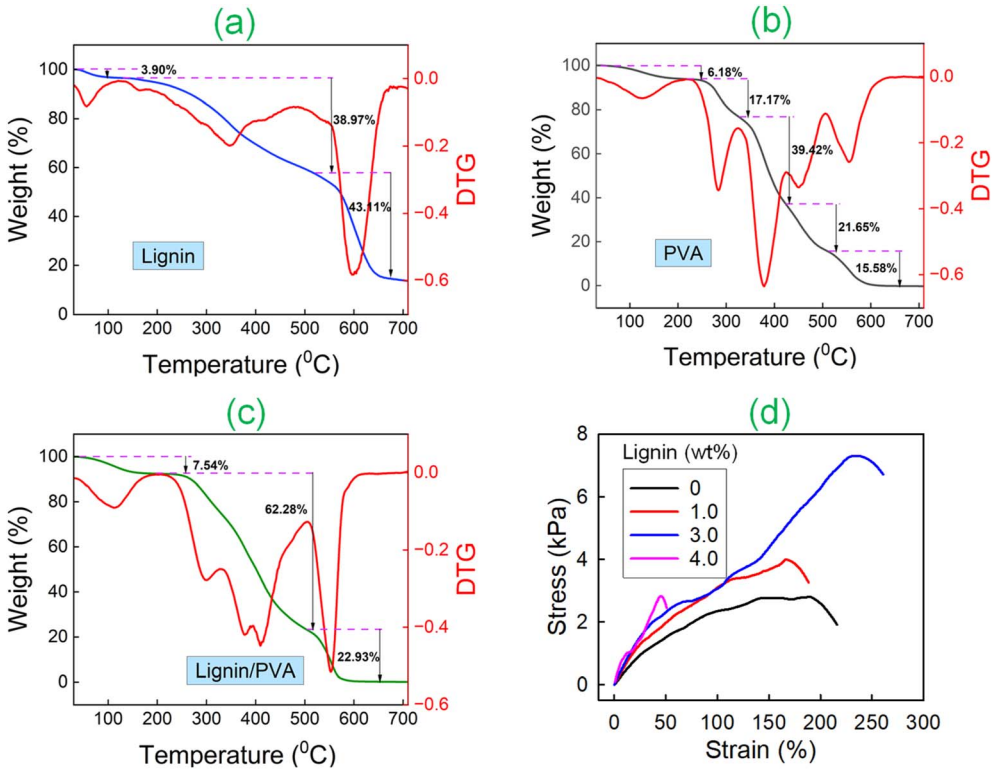

Fig. 5 TGA-DTG curves of (a) lignin, (b) PVA gel, and (c) lignin/PVA hydrogel. (d) Stress–strain curves of lignin/PVA hydrogels at various lignin contents.

Table 2. The pure PVA hydrogel exhibits moderate tensile strength and flexibility, characteristic of its soft polymeric network. Upon incorporation of lignin, a notable enhancement in mechanical performance is observed. The lignin/PVA hydrogel demonstrates a substantial improvement in mechanical performance. At low lignin concentrations (<3%), the limited number of interaction sites results in only marginal improvement in network strength compared to pure PVA. In contrast, the hydrogel containing 3% lignin exhibits optimal mechanical performance, demonstrating a well-balanced combination of strength and elasticity. However, at 4% and higher lignin contents, the hydrogel becomes brittle, as evidenced by a sharp decrease in elongation at break and toughness. This behavior is attributed to excessive lignin disrupting the homogeneity of the polymer network, leading to structural inhomogeneity and reduced flexibility. The improved mechanical properties at optimal lignin content can be attributed to a synergistic interaction between lignin and PVA. Lignin, a rigid aromatic biopolymer, acts as a reinforcing filler that enhances the stiffness and strength of the hydrogel matrix. Additionally, the presence of phenolic hydroxyl groups in lignin promotes strong intermolecular hydrogen bonding with the hydroxyl groups of PVA, facilitating efficient load transfer and improved network cohesion.[41,42] It is worth noting that while the fully swollen hydrogel exhibits relatively lower mechanical stability due to high water content, the as-prepared hydrogel containing 3% lignin demonstrates significantly superior mechanical performance (Fig. S3), with markedly higher tensile strength, modulus, and toughness (Table 2).

3.2 Adsorption of dyes by lignin/PVA hydrogel

The mechanically stable lignin/PVA hydrogel were employed as reusable adsorbents for removing CV and RhB dyes from their

Table 2 The mechanical properties of the lignin/PVA hydrogels at various lignin contents and the as-prepared hydrogel at 3% lignin

Lignin (%)	Young's modulus (kPa)	Tensile strength (kPa)	Strain at breaking (%)	Toughness (kJ m^{-3})
0.0	3.8	2.8	188.2	4.4
1.0	4.9	4.1	168.5	3.4
3.0	6.6	7.3	234.5	10.8
4.0	11.5	2.9	44.6	0.64
3.0[a]	30.2	50.8	331.2	72.6

[a] As-prepared lignin/PVA hydrogel.

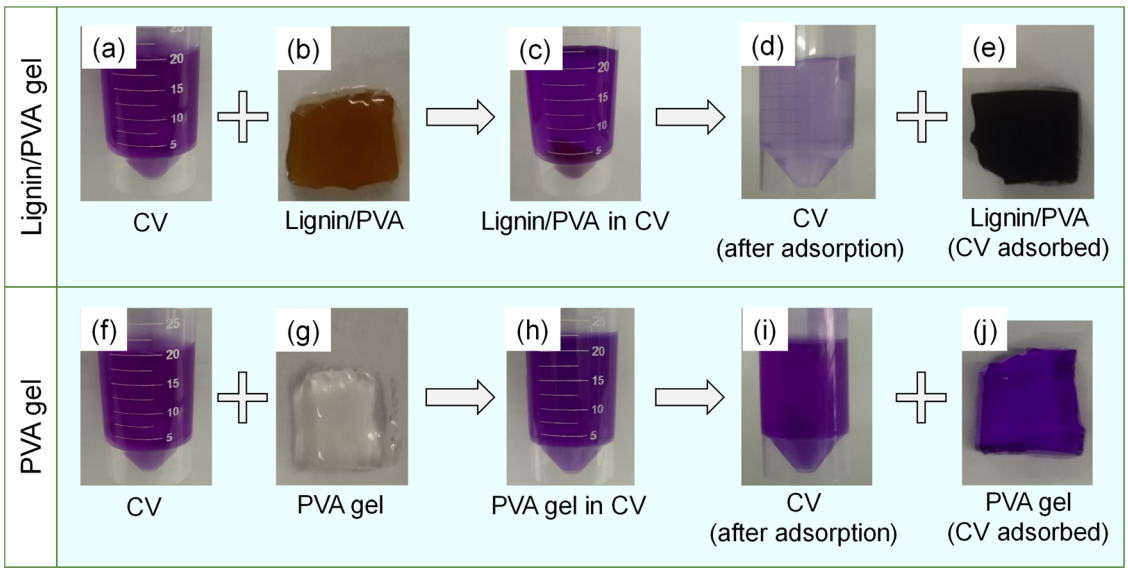

Fig. 6 Photographs to demonstrate the adsorption of CV dye by the lignin/PVA hydrogel (a–e) and PVA gel (f and g).

aqueous solutions, and the adsorption process is visually demonstrated in Fig. 6. The decolorization of the initially colored CV solution indicates the effective adsorption capacity of the hydrogel. As shown in Fig. 6a and b, the CV solution and lignin/PVA hydrogel appear unchanged prior to adsorption. Upon immersion of the hydrogel into the CV solution (Fig. 6c), a gradual color change is observed. During the adsorption process, the hydrogel darkens while the intensity of the violet color in the solution decreases, confirming dye uptake. After completion of the adsorption process, the hydrogel (Fig. 6e) can be easily separated from the treated solution (Fig. 6d), which becomes visibly decolorized. The darkened appearance of the hydrogel further confirms the successful adsorption of CV molecules. In contrast, the pure PVA hydrogel (Fig. 6f–j) exhibits negligible adsorption, as evidenced by the minimal change in solution color, highlighting the critical role of lignin incorporation in enhancing adsorption performance. Therefore, the lignin/PVA hydrogel not only exhibits high adsorption efficiency but also allows for easy post-treatment separation in practical wastewater treatment applications. Based on these results, further adsorption studies were conducted to optimize key parameters, such as effect of contact time, initial dye concentration, pH and adsorbent dosage, to achieve maximum removal performances.

3.2.1 Effect of contact time. The influence of contact time on the adsorption efficiency of CV and RhB dyes onto the lignin/PVA hydrogel was investigated under identical experimental conditions. A fixed adsorbent dosage (1.0 g of swollen hydrogel) was introduced into the dye solution, and the total volume was adjusted to 20 mL, yielding initial dye concentrations of 6×10^{-5} and 2×10^{-6} M for CV and RhB, respectively. The adsorption process was monitored over a period of 120 hours under static conditions (without mechanical stirring). As shown in Fig. 7a, both dyes exhibited a rapid adsorption phase (~50%) during the initial 24 hours, followed by a gradual decline in adsorption rate until the equilibrium is established at approximately 96 hours. This behavior suggests a two-stage adsorption mechanism: an initial fast surface adsorption driven by the availability of abundant active sites, followed by a slower diffusion-controlled phase in which dye molecules gradually penetrate into the internal pores of the hydrogel matrix. The relatively long equilibrium time can be attributed to the porous structure of the lignin/PVA hydrogel, which facilitates progressive intra-particle diffusion of dye molecules into the internal porous structure of the hydrogel.[43] The adsorption experiments under static condition was intentionally adopted to evaluate the intrinsic adsorption performance of the lignin/PVA hydrogel under a low-energy operation mode. While the longer equilibrium times required under static condition due to diffusion limitations, the feasibility of passive adsorption systems without external energy input provides insight into the low-energy industrial-scale applications. To investigate the effect of mechanical stirring during the adsorption process, additional experiments were conducted under identical condition with mechanical stirring [Fig. 7b]. Compared to static condition, stirring enhanced the adsorption rate, with ~80% removal of CV and ~60% removal of RhB achieved within 60 min due to faster mass transfer. This rapid uptake is attributed to reduced boundary layer thickness and improved external mass transfer. In contrast, the prolonged equilibrium time (~96 h) under static conditions indicates that intra-particle diffusion within the hydrogel matrix plays a dominant role. These results confirm that both external and internal diffusion processes govern the overall adsorption mechanism.

3.2.2 Effect of initial dye concentration. The effect of initial dye concentration on adsorption performance was assessed through batch experiments while keeping all other parameters constant [dosage of 1.0 g and contact time of 96 h] under static conditions. The initial concentration of CV was varied between 2×10^{-5} and 12×10^{-5} M, whereas that for RhB ranged from 1

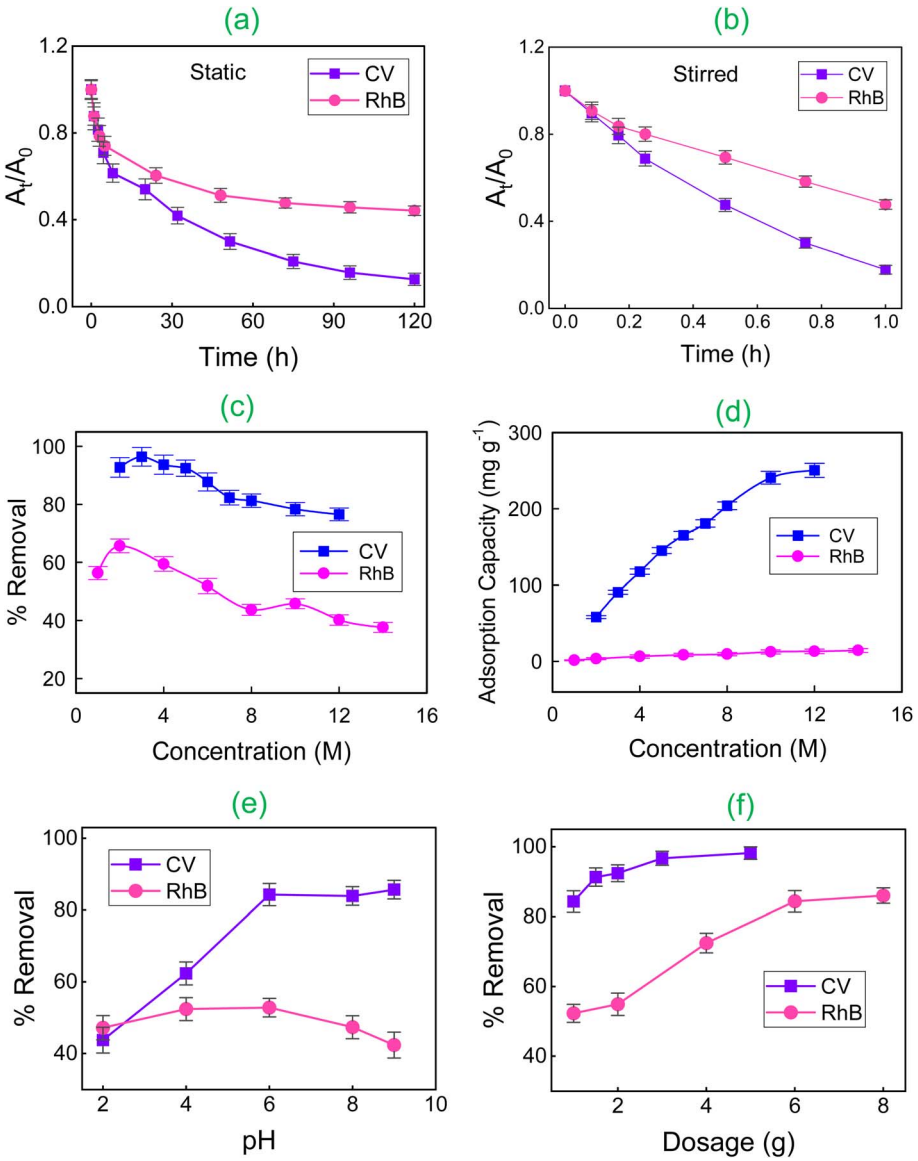

Fig. 7 The effect of contact time under static (a) and stirring condition (b) on the adsorption of CV and RhB by lignin/PVA hydrogel. The effect of initial dye concentration on the percent removal (c) and adsorption capacity (d). Percent removal of CV and RhB by lignin/PVA hydrogel at various pH (e) and adsorbent dose (f). The concentration of CV and RhB, shown in (c) and (d), are factorized by 10^{-5} and 10^{-6}, respectively.

$\times 10^{-6}$ M to 14 $\times 10^{-6}$ M. The results [Fig. 7c and d] demonstrate a clear dependence of adsorption behavior on the initial dye concentration. For both dyes, an increase in initial concentration initially led to a decrease in percent removal as well as the adsorption capacity, which can be attributed to the saturation of available active sites on the hydrogel surface.[44] At lower concentrations, a higher proportion of dye molecules can interact with abundant active sites, leading to greater removal efficiency. However, at higher concentrations, the number of dye molecules exceeds the available adsorption sites, resulting in reduced removal efficiency despite an increase in the adsorption capacity. The maximum removal efficiencies were observed at 3 $\times 10^{-5}$ M for CV and 2 $\times 10^{-6}$ M for RhB. Beyond these concentrations, a significant decline in removal percentage was observed while the maximum adsorption capacities reached to 250.9 mg g^{-1} for CV and 19.4 mg g^{-1} for RhB. Considering both adsorption capacity and removal efficiency, the optimal initial concentrations were considered as 6 $\times 10^{-5}$ M for CV and 2 $\times 10^{-6}$ M for RhB. These conditions provide a suitable balance between high dye uptake and effective removal performance.[45]

3.2.3 Effect of pH. The pH of the solution plays a crucial role in determining the surface charge of the adsorbent and the ionization state of dye molecules, thereby influencing the overall adsorption efficiency.[46] To investigate this effect, adsorption experiments were carried out by varying pH from 2 to 9 [Fig. 7e]. For CV, a cationic dye, adsorption efficiency increased significantly with increasing pH. At low pH, the phenolic –OH and other oxygen-containing functional groups in

lignin/PVA hydrogel matrix become protonated, resulting in a positively charged surface.[47] This leads to electrostatic repulsion between the positively charged adsorbent and the CV molecules, and further competition with excess H^+ ions for active sites, thereby reducing adsorption.[48] As the pH increases, deprotonation of these functional groups generates negatively charged sites, enhancing electrostatic attraction towards the cationic dye and significantly improving adsorption capacity.[49] Maximum adsorption of CV was observed at pH 9, suggesting dominating role of surface charge interactions. In contrast, RhB exhibits a more complex adsorption pattern due to its ability to exist in both cationic and zwitterionic forms depending on the pH. At pH < 3, RhB predominantly exists in its cationic form, which leads to electrostatic repulsion from the positively charged surface of the hydrogel, resulting in low adsorption efficiency.[50] As the pH increases, particularly at pH ∼ 6, RhB forms to its zwitterionic form, where it can engage in favorable interactions with the negatively charged functional groups on the hydrogel surface. At higher pH (>7), although the negative charge of the adsorbent increases, the affinity for RhB decreases due to complete conversion of its to zwitterionic form.[51] Maximum RhB adsorption was achieved at pH of 6, signifying the role of not only electrostatic interactions but also hydrophobic interactions and hydrogen bonding in the adsorption process.

3.2.4 Effect of adsorbent dose. The influence of adsorbent dose on dye removal efficiency was systematically investigated by varying the mass of lignin/PVA hydrogel from 1 to 8 g in 20 mL of dye solution, under otherwise constant conditions. As shown in Fig. 7f, higher adsorbent dose led to a significant enhancement in dye removal for both CV and RhB. This behavior is attributed to the greater availability of active binding sites and increased surface area with higher amounts of hydrogel, facilitating more dye molecules to be captured from the solution.[52] For CV, the removal efficiency increased sharply with adsorbent dose up to 3 g, beyond which only a marginal improvement was observed, indicating that most of the dye molecules had already been adsorbed. In contrast, RhB required a higher adsorbent dose (6 g) to achieve maximum removal efficiency which suggests a relatively weaker interaction between RhB molecules and the functional groups of hydrogel.

3.2.5 Effect of swelling ratio. The effect of swelling ratio (W_e/W_0) on the adsorption capacity of the lignin/PVA hydrogel are summarized in Table 3. The adsorption capacity significantly improved from 79.6 to 142.2 mg g^{-1} as the swelling ratio increased from 5.65 to 10.07. This enhancement can be attributed to the expansion of the hydrogel network, which increases pore accessibility and promotes diffusion of CV molecules into internal adsorption sites. At a swelling ratio of 10.07 (corresponding to 3% lignin), the hydrogel exhibits an optimal balance between network expansion and structural integrity, leading to efficient utilization of active sites. Under higher initial dye concentration, the same composition achieves a maximum adsorption capacity of 250.9 mg g^{-1}, confirming that the internal porous structure becomes highly accessible under favorable concentration gradients. However, a further increase in swelling ratio to 10.67 at 4% lignin results in a slight decline in adsorption capacity, which can be attributed to saturation of lignin incorporation within the hydrogel matrix. Therefore, an optimal balance between swelling and mechanical behavior is essential to achieve maximum adsorption performance.

3.3 Adsorption isotherm

To elucidate the adsorption behavior and underlying mechanism of dye uptake by the lignin/PVA hydrogel, the experimental data were analyzed using three widely applied isotherm models: Langmuir, Freundlich, and Temkin.[53] The corresponding isotherm model are presented in Fig. 8 and the calculated parameters are summarized in Table 4. The linear forms of Langmuir, Freundlich, and Temkin isotherm models are expressed by eqn (5)–(7).

$$\frac{C_e}{q_e} = \frac{1}{K_L Q_m} + \frac{C_e}{Q_m} \quad (5)$$

$$\ln q_e = \ln K_F + \frac{1}{n} \ln C_e \quad (6)$$

$$q_e = \frac{RT}{b} \ln K_T + \frac{RT}{b} \ln C_e \quad (7)$$

In eqn (5), q_e (mg g^{-1}) is the equilibrium adsorption capacity, C_e (mg L^{-1}) is the equilibrium concentration of the adsorbate, Q_m (mg g^{-1}) is the maximum adsorption capacity, and K_L (L mg^{-1}) is the Langmuir constant. While in eqn (6), K_F (mg g^{-1}) is the Freundlich constant associated with adsorption capacity, and $\frac{1}{n}$ is the heterogeneity factor indicating adsorption intensity. In eqn (7), K_T (L g^{-1}) and b (J mol^{-1}) represent equilibrium binding

Table 3 Adsorption capacity of the lignin/PVA hydrogel at various swelling ratio. Initial concentration of CV dye was taken as 6.0×10^{-5} M

Swelling ratio (W_e/W_0)	Swelling degree (W_e/W_{dry})	Lignin (%)	Adsorbent dose, W_e (g)	Adsorbent dose, W_{dry} (10^{-3} g)	Lignin, W_L (10^{-3} g)	Adsorption capacity (mg g^{-1})
5.65	62.62	1.0	1.0	15.97	1.77	79.6
7.63	76.26	2.0		13.11	2.62	123.8
10.07	91.75	3.0		10.90	2.97	142.2
10.07	91.75	3.0		10.90	2.97	250.9[a]
10.67	88.91	4.0		11.25	3.75	127.3

[a] The maximum adsorption capacity at initial CV dye concentration of 12.0×10^{-5} M.

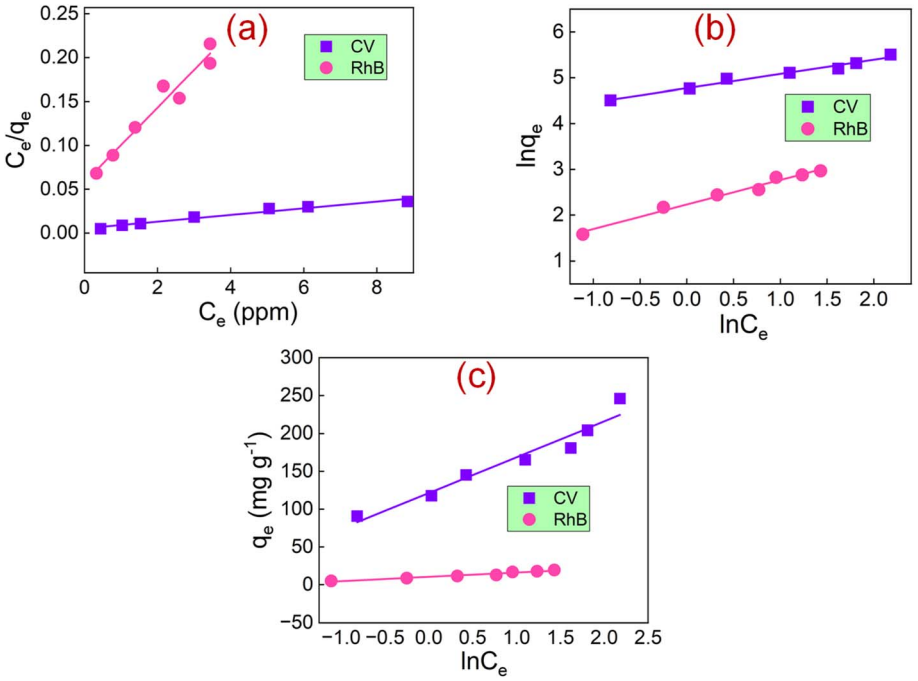

Fig. 8 Adsorption isotherms: (a) Langmuir, (b) Freundlich, and (c) Temkin model for CV and RhB dyes adsorption.

Table 4 Adsorption isotherm parameters for removal of CV and RhB by lignin/PVA hydrogel

	Adsorption isotherms					
Dye	Langmuir		Freundlich		Temkin	
CV	Q_m (mg g^{-1})	261.78	K_F (mg g^{-1})	118.32	K_T (L g^{-1})	13.03
	K_L (L mg^{-1})	1.37	$1/n$	0.3099	b (J mol^{-1})	52.42
	R^2	0.9588	R^2	0.9734	R^2	0.9320
	SSE	2533.29	SSE	2307.68	SSE	2402.23
	χ^2	23.78	χ^2	20.57	χ^2	20.62
RhB	Q_m (mg g^{-1})	23.39	K_F (mg g^{-1})	9.30	K_T (L g^{-1})	6.20
	K_L (L mg^{-1})	1.35	$1/n$	0.5371	b (J mol^{-1})	434.06
	R^2	0.9446	R^2	0.9783	R^2	0.9508
	SSE	13.66	SSE	8.10	SSE	4330.78
	χ^2	1.16	χ^2	1.25	χ^2	530.46

constant and Temkin isotherm constant associated with heat of adsorption, respectively.[54] To ensure a rigorous evaluation of model fitting, statistical error functions, including the sum of squared errors (SSE) and chi-square (χ^2), were considered alongside the correlation coefficient (R^2). Lower SSE and χ^2 values indicate better agreement between experimental and calculated data. The values of R^2, SSE, and χ^2 are included in Table 4. For CV adsorption, the Freundlich model exhibited the highest correlation coefficient ($R^2 = 0.973$) along with relatively lower error values (SSE = 2307.68, $\chi^2 = 20.57$) compared to the Langmuir model ($R^2 = 0.959$, SSE = 2533.29, $\chi^2 = 23.78$) and Temkin model ($R^2 = 0.932$, SSE = 2402.23, $\chi^2 = 20.62$). For RhB adsorption, the Freundlich model again showed the best fit with the highest R^2 (0.978) and the lowest SSE (8.10), while the Langmuir ($R^2 = 0.945$, SSE = 13.66, $\chi^2 = 1.16$) and Temkin ($R^2 = 0.951$, SSE = 4330.78, $\chi^2 = 530.46$) models showed comparatively poorer agreement. These results clearly demonstrate that the Freundlich isotherm model most appropriately describes the adsorption behavior of both dyes. This suggests that adsorption occurs on a heterogeneous surface with non-uniform energy distribution, involving multilayer adsorption mechanisms. In contrast, the Langmuir isotherm model, which assumes monolayer adsorption on a homogeneous surface,[55] did not adequately describe the system, indicating deviation from ideal monolayer behavior. In contrast, Freundlich isotherm model can describe both physisorption and chemisorption processes and implies multilayer adsorption on energetically heterogeneous surfaces. The relatively poorer fit of the Temkin model further suggests that the heat of adsorption does not vary linearly with surface coverage in this system.[56] On the other hand, the higher K_F value obtained for CV compared to RhB further indicates a greater adsorption affinity to the

hydrogel toward CV. Additionally, the $1/n$ values for both dyes are less than 1, confirming favorable interaction between the adsorbent and adsorbate.[57] Overall, the superior performance of the Freundlich model reflects the porous and heterogeneous nature of the lignin/PVA hydrogel, which facilitates efficient adsorption of dye molecules.

3.4 Adsorption kinetics

To investigate the rate-controlling mechanisms involved in the adsorption of crystal violet (CV) and rhodamine B (RhB) dyes onto the lignin/PVA hydrogel, experimental data were evaluated using pseudo-first-order, pseudo-second-order, and intra-particle diffusion models. The pseudo-first order equation can be expressed as:

$$\ln(q_e - q_t) = \ln q_e - K_1 t \quad (8)$$

where q_e and q_t denote amount of dye adsorbed (mg g^{-1}) in equilibrium and at time t, respectively. While K_1 is the pseudo-first order rate constant obtained from the slope of the plot $\ln(q_e - q_t)$ *vs.* t [Fig. 9a]. The linear form of pseudo-second order kinetic model is as follows:

$$\frac{t}{q_t} = \frac{1}{K_2 q_e^2} + \frac{t}{q_e} \quad (9)$$

In eqn (9), K_2 represents the pseudo-second order rate constant calculated from the intercept of the plot $\frac{t}{q_t}$ *vs.* t [Fig. 9b]. To assess whether diffusion within the pores was the rate-limiting step, the Weber–Morris intra-particle diffusion model was applied:

$$q_t = K_{id} t^{1/2} + C \quad (10)$$

where K_{id} and C are the intra-particle diffusion rate constant and intercept of the plot q_t *vs.* $t^{1/2}$ [Fig. 9c], respectively.[58] Among these models, both the pseudo-first-order and pseudo-second-order models exhibited good fits, as indicated by their high correlation coefficients (Table 5). However, pseudo-first-order model shows a slightly higher correlation coefficient (R^2 = 0.9956) compare to the pseudo-second-order model (R^2 = 0.9860) for CV adsorption. However, the difference in R^2 value is relatively small and model selection was not based solely on correlation coefficient. A more reliable criterion is the agreement between the calculated adsorption capacity ($q_{e,cal}$) and the experimental value ($q_{e,exp}$). For the pseudo-first-order model, a significant deviation was observed between $q_{e,cal}$ (171.5 mg g^{-1}) and $q_{e,exp}$ (~211 mg g^{-1}) for CV adsorption, indicating that this model does not adequately describe the adsorption process. In contrast, the pseudo-second-order model provides much closer agreement ($q_{e,cal}$ = 219.3 mg g^{-1}) with the experimental value. Therefore, the pseudo-second-order model is considered more appropriate for describing the adsorption kinetics of CV, suggesting that chemisorption involves in the adsorption process. On the other hand, the higher correlation coefficient and closer agreement with experimental values (Table 5) revealed that the pseudo-second-order model is considered more appropriate for describing the adsorption of RhB. The rate constants (K_2) for pseudo-second-order

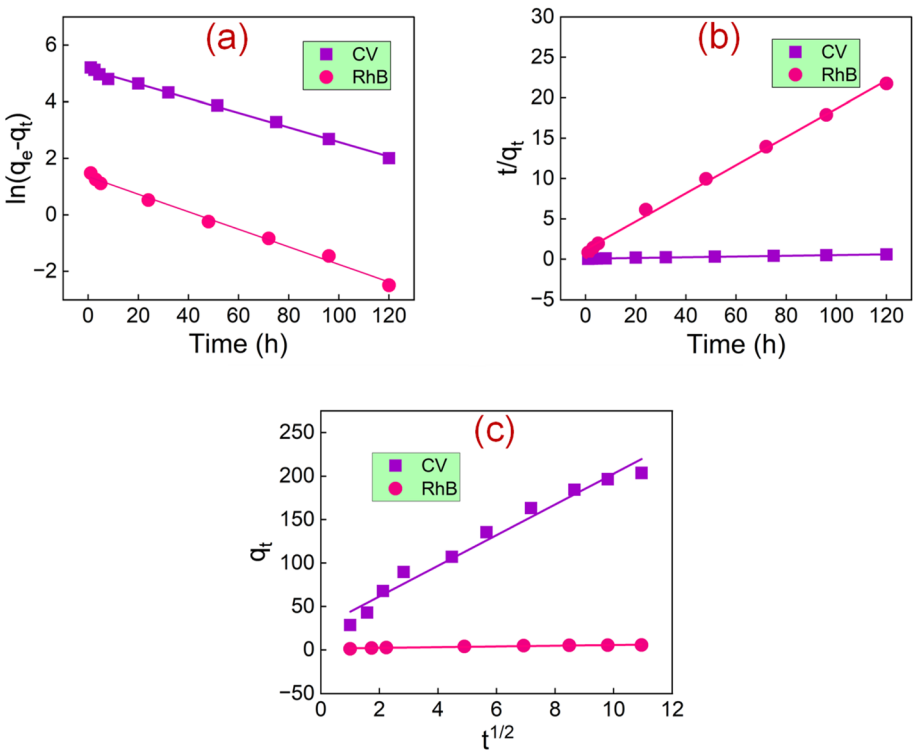

Fig. 9 Adsorption kinetics for the (a) pseudo-first order, (b) pseudo-second order, and (c) intra-particle diffusion model.

Table 5 Parameters for kinetic studies of CV and RhB dyes adsorption on lignin/PVA hydrogel

	Adsorption kinetics					
Dye	Pseudo-first order		Pseudo-second order		Intra particle diffusion	
CV	q_e (mg g^{-1})	171.5	q_e (mg g^{-1})	219.3	K_{id} (mg g^{-1} h^{-1})	17.6
	K_1 (h^{-1})	0.0257	K_2 (g mg^{-1} h^{-1})	0.0003	C	26.3283
	R^2	0.9956	R^2	0.9860	R^2	0.9320
RhB	q_e (mg g^{-1})	3.87	q_e (mg g^{-1})	5.73	K_{id} (mg g^{-1} h^{-1})	0.42
	K_1 (h^{-1})	0.0312	K_2 (g mg^{-1} h^{-1})	0.0256	C	1.4201
	R^2	0.9922	R^2	0.9966	R^2	0.9290

adsorption were 0.0003 g mg^{-1} h^{-1} for CV and 0.0256 g mg^{-1} h^{-1} for RhB. The intra-particle diffusion plots did not pass through the origin, denoting that although intra-particle diffusion contributes to the overall adsorption, it is not the sole rate-limiting step.[59] These findings suggest that the adsorption of both dyes is better described by the pseudo-second order kinetic model, implying that chemisorption contributes to the adsorption process. In this model, the adsorption rate is controlled by both the amount of dye adsorbed onto the hydrogel and the concentration of dye remaining in the solution.[60]

3.5 Thermodynamic study

The thermodynamic parameters for the adsorption of CV and RhB onto the lignin/PVA hydrogel were evaluated to understand the feasibility, spontaneity, and nature of the adsorption process. The standard thermodynamic parameters, including Gibbs free energy change (ΔG°), enthalpy change (ΔH°), and entropy change (ΔS°), were determined by using the following equations:

$$\Delta G^\circ = -RT \ln K_c \quad (11)$$

$$\Delta G^\circ = \Delta H^\circ - T\Delta S \quad (12)$$

$$\ln K_c = -\frac{\Delta H^\circ}{RT} + \frac{\Delta S^\circ}{R} \quad (13)$$

where, K_c ($=q_e/C_e$) is the concentration equilibrium constant, T is the temperature, and R is the universal gas constant.[61] The Van't Hoff plots of $\ln K_c$ *versus* $1/T$ for both CV and RhB exhibited good linearity (Fig. S4), indicating the applicability of the thermodynamic model. The values of ΔH° and ΔS° were obtained from the slope and intercept, respectively, while ΔG was calculated using eqn (12). The obtained thermodynamic parameters are summarized in Table 6. The negative values of ΔG° at all studied temperatures confirm confirmed the spontaneous nature of adsorption for both dyes, with more negative values observed for CV, indicating stronger interaction with the adsorbent. The increase in the magnitude of ΔG° with temperature further suggested that the adsorption process is favored at higher temperatures. The positive ΔH° values for both CV (~32 kJ mol^{-1}) and RhB (~27 kJ mol^{-1}) indicated that the adsorption process is endothermic in nature. The relatively higher ΔH° value for CV implies stronger adsorbate–adsorbent interactions compared to RhB. Additionally, the positive ΔS° values for both dyes suggested increased randomness at the solid–liquid interface during adsorption, likely due to the displacement of water molecules by dye species within the hydrogel matrix. The higher ΔS° value observed for CV further supports its greater affinity towards the adsorbent. Overall, the relatively low negative ΔG° values (−2.98 to −8.10 kJ mol^{-1}) suggest that the adsorption process is spontaneous and physisorption plays a significant role. However, the moderate ΔH° values (27–32 kJ mol^{-1}), along with pseudo-second-order kinetics and possible nature of interactions (hydrogen bonding and π–π interactions), suggest that chemisorption contributes to the overall adsorption process alongside physisorption. The comparatively lower values of thermodynamic parameters for RhB can be attributed to its larger molecular size and partial zwitterionic nature, which hinder its diffusion into the porous structure and reduce its interaction with active sites compared to CV.

Table 6 Standard thermodynamic parameters for adsorption of CV and RhB onto lignin/PVA hydrogel

Dye	T (K)	K_c	ΔG° (kJ mol^{-1})	ΔH° (kJ mol^{-1})	ΔS° (J mol^{-1} K^{-1})
CV	298	6.00	−4.33	31.7	120.8
	308	8.25	−5.53		
	318	12.00	−6.74		
	328	19.50	−7.95		
RhB	298	3.33	−2.93	27.1	100.8
	308	4.53	−3.94		
	318	6.25	−4.94		
	328	9.11	−5.95		

3.6 Significance of hydrogel formation in enhancing adsorption performance

The synthesis of the lignin/PVA hydrogel was essential to achieve effective dye adsorption, as it combined the advantageous properties of both materials. lignin, rich in aromatic rings and negatively charged functional groups (*e.g.*, phenolic –OH), possesses inherent affinity toward cationic dyes like CV and RhB. However, in its native or bulk form, lignin tends to aggregate, limiting the availability of active adsorption sites.[62] On the other hand, only PVA gel provides a stable polymeric matrix but lacks sufficient functional groups and surface affinity for efficient dye adsorption.[63] By incorporating lignin

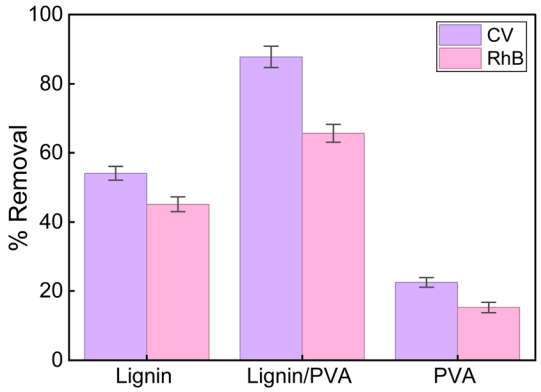

Fig. 10 Comparison of removal efficiencies of lignin, PVA hydrogel and lignin/PVA hydrogel.

into the PVA hydrogel matrix, the structure allowed for better dispersion of lignin molecules, thereby increasing the accessibility of aromatic and negatively charged sites. This synergistic integration improved the hydrogels adsorption capacity by preventing lignin aggregation and enhancing the surface area and porosity.[64] Experimental removal efficiencies showed in Fig. 10 confirms that the lignin/PVA hydrogel exhibited the highest adsorption efficiency for both CV and RhB dyes, significantly outperforming pure lignin and PVA gel.

3.7 Adsorption mechanism

The adsorption mechanism of CV and RhB dyes onto the lignin/PVA hydrogel can be understood based on morphological and spectroscopic analyses. SEM images revealed that the lignin/PVA hydrogel possesses a rough and porous surface, which significantly enhances the surface area and provides abundant adsorption sites. Scheme 2 shows adsorption of both dyes onto hydrogel. The adsorption process involves both surface and pore diffusion mechanisms. Due to the porous nature of the hydrogel, dye molecules can penetrate into internal cavities and bind to available functional groups. This structural feature supports multilayer adsorption behavior, consistent with the Freundlich isotherm model, which reflects adsorption on heterogeneous surfaces. CV dye, being smaller in molecular size compared to RhB, more readily enters the pores and establishes interactions within the internal matrix, resulting in higher adsorption capacity.[65]

FT-IR spectra of the hydrogel confirmed the presence of functional groups from lignin, such as phenolic –OH, methoxy, and aromatic rings, all of which play crucial roles in dye binding. A proposed adsorption mechanism for binding of CV and RhB dyes onto lignin involves multiple interaction forces (Scheme 3). The negatively charged functional groups on lignin, such as deprotonated –OH, engage in electrostatic interactions with the positively charged nitrogen atoms in CV and RhB dyes. Additionally, hydrogen bonding occurs between the hydroxyl groups of lignin and functional groups on the dyes. π–π interactions between the aromatic rings of lignin and those of the dyes further stabilize the adsorption complex.[66,67] The FT-IR spectra of the lignin/PVA hydrogel before and after adsorption [Fig. S5(a and b)] were compared to elucidate the adsorption mechanism. After adsorption, the O–H stretching band exhibited a shift toward lower wavenumbers, indicating the

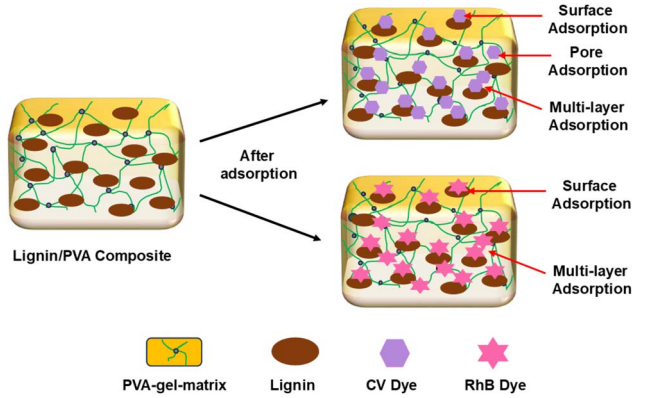

Scheme 2 Mechanism of CV and RhB dyes adsorption into lignin/PVA hydrogel.

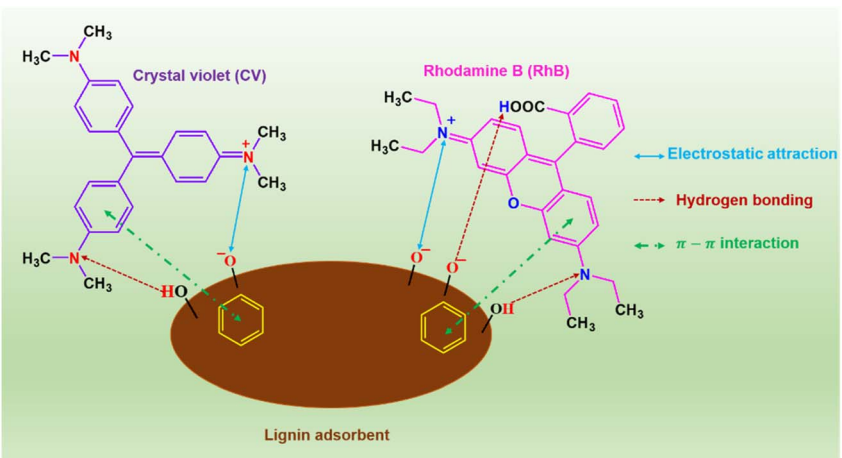

Scheme 3 Possible interactions of CV and RhB dyes with lignin adsorbent.

formation of hydrogen bonding interactions between hydroxyl groups of the adsorbent and dye molecules. In addition, changes in the aromatic C=C stretching peaks were observed, suggesting the involvement of π–π interactions between lignin aromatic rings and the conjugated structures of CV and RhB. Therefore, the adsorption of CV and RhB onto lignin/PVA hydrogels is likely governed by a combination of electrostatic attraction, hydrogen bonding, and π–π interactions. These findings are consistent with the kinetic and thermodynamic analyses, further supporting the involvement of both physical and chemical interaction.

3.8 Reusability of lignin/PVA hydrogel adsorbent

In practical wastewater treatment applications, the reusability of an adsorbent is a critical factor that determines its industrial viability and cost-effectiveness.[68] To evaluate the regeneration potential of the synthesized lignin/PVA hydrogel, adsorption–desorption cycles were carried out for up to five consecutive runs. The adsorbed dyes, CV and (RhB), were desorbed using a simple washing procedure involving ethanol and deionized water, without the need for drying or complex treatment steps. This straightforward regeneration process demonstrates a clear operational advantage over many conventional adsorbents that require energy-intensive drying or chemical reactivation steps. The lignin/PVA hydrogel was easily separable from solution due to its stable, solid structure, allowing for rapid collection and reuse. To quantitatively evaluate the regeneration performance of the lignin/PVA hydrogel, the regeneration efficiency (%) was also calculated using the relation: regeneration efficiency (%) = $(q_n/q_1) \times 100$, where q_1 and q_n represent the adsorption capacities in the first and subsequent cycles, respectively. As shown in Fig. 11, the lignin/PVA hydrogel exhibited high dye removal efficiency, adsorption capacity, and regeneration efficiency over successive multiple adsorption–desorption cycles for CV. Although a gradual decline was observed after each cycle, regeneration efficiency of the hydrogel retained above 81% of its initial adsorption performances, indicating good structural stability and reusability of the hydrogel. The decrease in adsorption capacity over cycles is mainly attributed to the incomplete desorption under static regeneration conditions, progressive occupation or blockage of active sites, and possible structural relaxation of the hydrogel network upon repeated use.[69] Post cycling FT-IR [Fig. S5(c)] of lignin/PVA hydrogel were compared with that of the pristine hydrogel (Fig. S5a) and post adsorption (Fig. S5b) to elucidate the regeneration and gradual decline of adsorption performance. After regeneration, the characteristic bands (O–H, C=C, and C–O) partially return toward their original positions, indicating partial recovery of the hydrogel structure. However, slight deviations remain, suggesting incomplete desorption and gradual modification of active sites, which may contribute to the observed decline in adsorption performance over repeated cycles. In addition, the incomplete desorption of the adsorbed dye may arise due to perform the desorption process by soaking the dye-adsorbed hydrogel in ethanol under static condition. Optimization of the desorption process under mechanical stirring, including

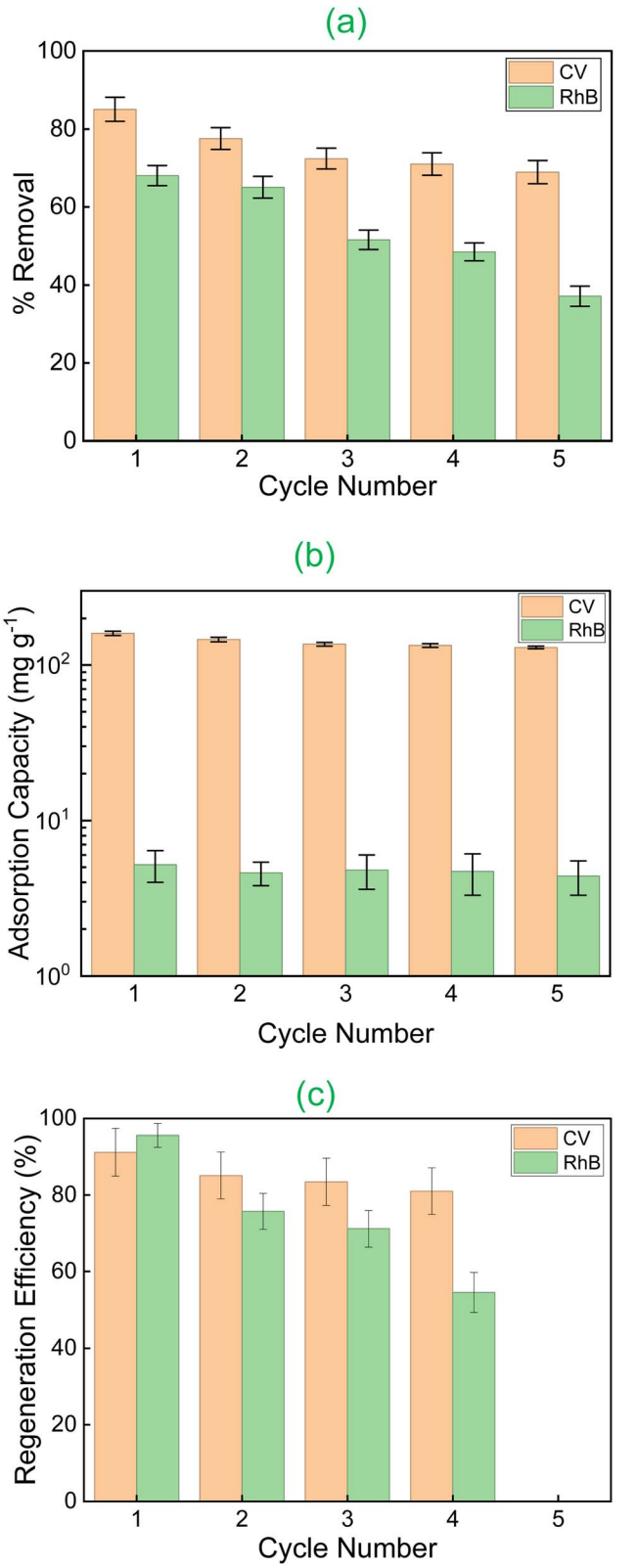

Fig. 11 Regeneration performance of lignin/PVA hydrogel over five successive adsorption–desorption cycles for the adsorption of CV and RhB dyes: (a) % removal, (b) adsorption capacity, and (c) regeneration efficiency.

Table 7 Comparative analysis of adsorption capacities of various lignin-based adsorbents for dye removal

Adsorbent	Source of lignin	Dye	Adsorption capacity (mg g^{-1})	Ref.
Lignin/cellulose hydrogel	Commercial	Congo red	294.0	70
		Malachite green	129.8	
Lignin copper ferrite	Agro-industrial	Crystal violet	34.1	48
Acrylic lignosulfonate resin	Commercial	Crystal violet	150.4	72
Lignin/PVA hydrogel	Industrial by-product	Crystal violet	169.0	23
		Rhodamine 6G	196.0	
		Methylene blue	179.0	
Lignin/PVA hydrogel	Commercial	Crystal violet	190.0	71
		Methylene blue	193.0	
Lignin/PVA hydrogel	**Waste liquor**	**Crystal violet**	**250.9**	**This work**

eluent selection and operational conditions, would be crucial to improve the reusability of the hydrogel. Overall, the lignin/PVA hydrogel exhibits excellent reusability, confirming its potential as a durable and sustainable adsorbent for repeated use in dye removal from industrial wastewater.

3.9 Comparison study

The adsorption performance of the synthesized lignin/PVA hydrogel was evaluated in comparison with previously reported lignin-based adsorbents to assess its effectiveness and advancement (Table 7). Lignin-based materials have been widely investigated for dye removal due to their abundant functional groups and aromatic structures. However, their adsorption performance varies significantly depending on composition, crosslinking strategy, and structural design. For example, lignin/cellulose hydrogels exhibit high adsorption capacities (294 mg g^{-1}) for anionic dyes such as Congo red, but show comparatively lower efficiency toward cationic dyes, malachite green.[70] In contrast, lignin/PVA hydrogels have been reported to achieve adsorption capacities of 169–190 mg g^{-1} for cationic dyes, CV.[23,71] Similarly, other lignin-derived adsorbents, such as lignin–metal oxide composites or chemically modified lignin resins, typically achieve moderate adsorption capacities (*e.g.*, ~34–150 mg g^{-1} for CV), often requiring additional functionalization steps or complex synthesis routes.[48,72]

In this study, the prepared lignin/PVA hydrogel exhibits a relatively high adsorption capacity for cationic CV (250.9 mg g^{-1}). Higher adsorption capacities (294 mg g^{-1}) have been reported by Li *et al.*;[70] however, their system involves lignin derived from a commercial source and targets an anionic dye. On the other hand, industrial waste-derived lignin/PVA hydrogels reported by Wu *et al.*,[23] show weak adsorption performance (169 mg g^{-1}) toward CV. In contrast, the present hydrogel, synthesized using agro-industrial waste-derived lignin, demonstrates excellent performance toward cationic dye adsorption. These results highlight that comparable or even superior adsorption efficiency can be achieved using low-cost, waste-derived lignin without the need for highly refined starting materials.

Compared with many highly engineered lignin-based hydrogels, which require complex chemical functionalization, the present hydrogel offers a simpler and more sustainable synthesis approach using waste-black-liquor-derived lignin. This approach minimizes processing complexity while still achieving competitive adsorption performance, particularly for CV dye adsorption. Under static conditions, the hydrogel exhibited a relatively long equilibrium time (~96 h). However, under stirring conditions, the equilibrium time significantly reduced to ~1 h due to enhanced mass transfer and reduced boundary layer resistance around the hydrogel surface. This highlights that hydrogel possesses strong intrinsic adsorption capability, while mass transfer limitations within the bulk hydrogel structure influence the overall kinetics. Similar adsorption behavior has also been reported for other hydrogel-based adsorbent systems in the literature. Importantly, this study distinguishes itself by establishing a clear relationship between network structure, swelling behavior, mechanical stability, and adsorption performance. These findings provide valuable insight into the rational design and optimization of sustainable lignin-based hydrogel adsorbents derived from industrial waste streams for wastewater treatment applications.

4. Conclusions

In this study, lignin was successfully extracted from black liquor, a waste generated in pulp and paper processing, and incorporated in poly(vinyl alcohol) (PVA) matrix by a one-pot crosslinking reaction using epichlorohydrin to develop a lignin/PVA hydrogel. The synthesized hydrogel demonstrated excellent adsorption performance for removal CV and RhB dyes from aqueous solutions. The enhanced adsorption behavior can be attributed to the synergistic integration of lignin and PVA, where lignin provides aromatic structures and negatively charged functional groups, while the PVA network offers a porous and flexible framework. This combination facilitates efficient adsorption, with a stronger affinity observed for CV due to its favorable molecular characteristics and stronger electrostatic interactions. Isotherm, kinetic and thermodynamic analyses revealed that the adsorption process follows the Freundlich model and pseudo-second-order kinetics, indicating multilayer adsorption on a heterogeneous surface, with contributions from both physisorption and chemisorption. In addition, the hydrogel exhibits improved mechanical strength, structural stability, and easy separation from aqueous media,

making it suitable for repeated use in industrial applications. Overall, this study demonstrates that waste-derived lignin can be effectively utilized to develop a cost-effective and sustainable hydrogel adsorbent with competitive performance. The findings provide valuable insights into the design of lignin-based materials for wastewater treatment and highlight a promising waste-to-value strategy for lignin utilization.

Author contributions

U. T. Jannat: writing – original draft, validation, resources, methodology, investigation, formal analysis, data curation. M. A. Haque: writing – review and editing, supervision, project administration, methodology. S. A. Aumi: characterization, formal analysis, data curation. S. K. Ray: characterization, methodology, formal analysis. M. Moniruzzaman: characterization, methodology, formal analysis. M. S. Jahan: data curation, characterization, M. A. A. Shaikh: data curation, characterization. M. Q. Ehsan: supervision, methodology, formal analysis, data curation.

Conflicts of interest

There are no conflicts of interest to declare.

Data availability

The data supporting the findings of this study are available within the article and the supplementary information (SI) file. Raw data are available from the corresponding author (anamul@du.ac.bd) upon reasonable request. Supplementary information is available. See DOI: https://doi.org/10.1039/d6ra01545j.

Acknowledgements

This research was primarily supported by the UGC Research Grant (2024–25), University of Dhaka, Bangladesh. This study was partially supported by the Special Research Grants (2023–24: Project ID: SRG-236687), Ministry of Science & Technology Bangladesh.

References

1 M. Musa, Y. Gao, P. Rahman, A. Albattat, M. A. S. Ali and S. K. Saha, *Clean Technol. Environ. Policy*, 2024, **26**, 1799–1823.
2 Y. Dinakarkumar, G. Ramakrishnan, K. R. Gujjula, V. Vasu, P. Balamurugan and G. Murali, *Environ. Chem. Ecotoxicol.*, 2024, **6**, 293–302.
3 S. Afroze and T. K. Sen, *Water, Air, Soil Pollut.*, 2018, **229**, 225.
4 B. S. Rathi, P. S. Kumar and D.-V. N. Vo, *Sci. Total Environ.*, 2021, **797**, 149134.
5 C. Yang, Q. Yao, L. Li, X. Xiao, L. Lu, C. Liu, C. Zhu, S. Zhan and H. Yuan, *Appl. Catal., B*, 2025, **366**, 125056.
6 Y. Fang, Q. Wu, X. Ma and Z. Ren, *CrystEngComm*, 2025, **27**, 4555–4567.
7 K. F. Kayani, S. J. Mohammed, M. S. Mustafa and S. B. Aziz, *Mater. Adv.*, 2025, **6**, 5391–5409.
8 S. Mani and R. N. Bharagava, Exposure to crystal violet, its toxic, genotoxic and carcinogenic effects on environment and its degradation and detoxification for environmental safety, in *Reviews of Environmental Contamination and Toxicology*, ed. W. de Voogt, Springer International Publishing, Cham, 2016, vol. 237, pp. 71–104.
9 A. A. Al-Gheethi, Q. M. Azhar, P. Senthil Kumar, A. A. Yusuf, A. K. Al-Buriahi, R. M. S. Radin Mohamed and M. M. Al-shaibani, *Chemosphere*, 2022, **287**, 132080.
10 W. Sun, C. Su, W. Zhang, H. Li, H. Zhao and R. Chen, *J. Environ. Chem. Eng.*, 2025, **13**, 117428.
11 P. S. Priya, P. Pratiksha Nandhini, S. Vaishnavi, V. Pavithra, M. H. Almutairi, B. O. Almutairi, S. Arokiyaraj, R. Pachaiappan and J. Arockiaraj, *Comp. Biochem. Physiol., Part C:Toxicol. Pharmacol.*, 2024, **280**, 109898.
12 G. Sudarjanto, B. Keller-Lehmann and J. Keller, *J. Hazard. Mater.*, 2006, **138**, 160–168.
13 H. R. Rashidi, N. M. N. Sulaiman, N. A. Hashim, C. R. C. Hassan and M. R. Ramli, *Desalin. Water Treat.*, 2015, **55**, 86–95.
14 S. Sonal and B. K. Mishra, in *Water Pollution and Management Practices*, Springer Singapore, Singapore, 2021, pp. 303–331.
15 O. Türgay, G. Ersöz, S. Atalay, J. Forss and U. Welander, *Sep. Purif. Technol.*, 2011, **79**, 26–33.
16 R. Chikri, N. Elhadiri, M. Benchanaa and Y. El maguana, *J. Chem.*, 2020, **2020**, 1–17.
17 V. K. Gupta and Suhas, *J. Environ. Manage.*, 2009, **90**, 2313–2342.
18 M. T. Yagub, T. K. Sen, S. Afroze and H. M. Ang, *Adv. Colloid Interface Sci.*, 2014, **209**, 172–184.
19 F. Elbehiry, T. Alshaal, N. Elhawat and H. Elbasiouny, Environmental-friendly and cost-effective agricultural wastes for heavy metals and toxicants removal from wastewater, in *Cost-Efficient Wastewater Treatment Technologies: Natural Systems*, Springer International Publishing, Cham, Switzerland, 2021, pp. 107–127.
20 J. Rajesh Banu, S. Kavitha, R. Yukesh Kannah, T. Poornima Devi, M. Gunasekaran, S.-H. Kim and G. Kumar, *Bioresour. Technol.*, 2019, **290**, 121790.
21 S. Sharma, A. Sharma, S. I. Mulla, D. Pant, T. Sharma and A. Kumar, Lignin as potent industrial biopolymer: an introduction, in *Lignin*, ed. S. Sharma and A. Kumar, *Springer Series on Polymer and Composite Materials*, Springer, Cham, 2020.
22 T. Wang, Z. Liu, P. Li, H. Wei, K. Wei and X. Chen, *Chem. Eng. J.*, 2023, **466**, 143118.
23 L. Wu, S. Huang, J. Zheng, Z. Qiu, X. Lin and Y. Qin, *Int. J. Biol. Macromol.*, 2019, **140**, 538–545.
24 X. Zhao, H. Zhao, A. Mei, L. Peng and J. Sun, *Int. J. Biol. Macromol.*, 2025, **285**, 138177.
25 X. Li, Q. Xia, Y. Leng, X. Cai and D. Nie, *Langmuir*, 2025, **41**, 16506–16518.
26 A. K. Sonker, K. Rathore, A. K. Teotia, A. Kumar and V. Verma, *J. Appl. Polym. Sci.*, 2019, **136**, 47393.

27 K. Koljonen, M. Österberg, M. Kleen, A. Fuhrmann and P. Stenius, *Cellulose*, 2004, **11**, 209–224.
28 C. Mancera, F. Ferrando, J. Salvadó and N. E. El Mansouri, *Biomass Bioenergy*, 2011, **35**, 2072–2079.
29 S. Tan, A. Blencowe, K. Ladewig and G. G. Qiao, *Soft Matter*, 2013, **9**, 5239.
30 Q. Lv, M. Wu and Y. Shen, *Colloids Surf., A*, 2019, **583**, 123972.
31 H. Patel, *Int. J. Environ. Sci. Technol.*, 2022, **19**, 10409–10426.
32 S. Yadav, A. Asthana, A. K. Singh, R. Chakraborty, S. S. Vidya, M. A. B. H. Susan and S. A. C. Carabineiro, *J. Hazard. Mater.*, 2021, **409**, 124840.
33 H. Hatakeyama and T. Hatakeyama, in *Biopolymers: Lignin, Proteins, Bioactive Nanocomposites*, ed. A. Abe, K. Dusek and S. Kobayashi, Springer, Berlin, Heidelberg, 2009, vol. 232, pp. 1–63.
34 K. Chang, *Carbohydr. Polym.*, 2000, **43**, 163–169.
35 X. Lin, J. Zhang, H. Feng and C. Xue, *Colloid Polym. Sci.*, 2023, **301**, 93–105.
36 J. Yao, K. Odelius and M. Hakkarainen, *Funct. Compos. Mater.*, 2020, **1**, 5.
37 J. Umeda, M. Kawakami, K. Kondoh, E.-S. Ayman and H. Imai, *Mater. Chem. Phys.*, 2010, **123**, 649–657.
38 A. G. Barneto, C. Vila and J. Ariza, *Thermochim. Acta*, 2011, **520**, 110–120.
39 W. Li, F. Xue and R. Cheng, *Front. Chem.*, 2007, **2**, 188–192.
40 Y. Wang, S. Liu, Q. Wang, X. Fu and P. Fatehi, *Cellulose*, 2020, **27**, 8725–8743.
41 J. Sun, C. Wang, J. C. C. Yeo, D. Yuan, H. Li, L. P. Stubbs and C. He, *Macromol. Mater. Eng.*, 2016, **301**, 328–336.
42 S. Zhang, M. Li, N. Hao and A. J. Ragauskas, *ACS Omega*, 2019, **4**, 20197–20204.
43 K.-J. Hwang, W.-G. Shim, Y. Kim, G. Kim, C. Choi, S. O. Kang and D. W. Cho, *Phys. Chem. Chem. Phys.*, 2015, **17**, 21974–21981.
44 Z. Eren and F. N. Acar, *Desalination*, 2006, **194**, 1–10.
45 A. Sharma, S. Datta, R. K. Sanjana, B. M. Pooja, S. Bose and G. Hegde, *RSC Adv.*, 2025, **15**, 7786–7798.
46 H. Hu, J. Li and S. Wu, *Sustainability*, 2022, **15**, 375.
47 R. M. Ali, H. A. Hamad, M. M. Hussein and G. F. Malash, *Ecol. Eng.*, 2016, **91**, 317–332.
48 R. Ali, Z. Elsagan and S. AbdElhafez, *Molecules*, 2022, **27**, 1831.
49 L. M. Cotoruelo, M. D. Marqués, F. J. Díaz, J. Rodríguez-Mirasol, J. J. Rodríguez and T. Cordero, *Environ. Prog. Sustainable Energy*, 2012, **31**, 386–396.
50 O. S. Bello, E. O. Alabi, K. A. Adegoke, S. A. Adegboyega, A. A. Inyinbor and A. O. Dada, *Heliyon*, 2020, **6**, e02872.
51 A. A. Inyinbor, F. A. Adekola and G. A. Olatunji, *Appl. Water Sci.*, 2017, **7**, 2297–2307.
52 N. Y. Nguyen-Thi, C. Q. Nguyen, Q. Le Dang, Q. De Tran, T. N. Do-Thi and L. H. Vu Thanh, *RSC Adv.*, 2024, **14**, 4533–4542.
53 S. Mallakpour and M. Naghdi, *New J. Chem.*, 2020, **44**, 11566–11576.
54 A. M. E. Mohammed, A. Kotb, M. M. S. Sanad, M. Abdel-Hakim and A. S. A. Ahmed, *RSC Adv.*, 2024, **14**, 31332–31347.
55 S. I. Al-Saeedi, A. Areej, M. T. Qamar, A. Alhujaily, S. Iqbal, M. T. Alotaibi, M. Aslam, M. A. Qayyum, A. Bahadur, N. S. Awwad, Y. Jazaa and E. B. Elkaeed, *Front. Environ. Sci.*, 2023, **11**, 1156475.
56 K. H. Chu, *Ind. Eng. Chem. Res.*, 2021, **60**, 13140–13147.
57 H. Freundlich, *Z. Phys. Chem.*, 1907, **57**, 385–470.
58 D. M. R. E. A. Dissanayake, W. M. K. E. H. Wijesinghe, S. S. Iqbal, N. Priyantha and M. C. M. Iqbal, *RSC Adv.*, 2016, **6**, 98682–98692.
59 J. Saikia, Y. Sikdar, B. Saha and G. Das, *J. Environ. Chem. Eng.*, 2013, **1**, 1166–1173.
60 Y.-S. Ho, *Adsorption*, 2004, **10**, 151–158.
61 M. M. Yunus and B. G. Gumau, *Int. J. Res. Sci. Innov.*, 2021, **08**, 195–200.
62 C. Song, C. Gao, P. Fatehi, S. Wang, C. Jiang and F. Kong, *Int. J. Biol. Macromol.*, 2023, **240**, 124368.
63 S. R. Sandeman, V. M. Gun'ko, O. M. Bakalinska, C. A. Howell, Y. Zheng, M. T. Kartel, G. J. Phillips and S. V. Mikhalovsky, *J. Colloid Interface Sci.*, 2011, **358**, 582–592.
64 J. Yang, D. Chen, Y. Zhu, Y. Zhang and Y. Zhu, *Appl. Catal., B*, 2017, **205**, 228–237.
65 Y. Wang, L.-P. Fang, H.-Y. Zhang, J.-J. Ren, T. Liang, X.-B. Lv, C.-J. Cheng and H.-R. Yu, *Int. J. Biol. Macromol.*, 2024, **278**, 134457.
66 C. Poornachandhra, R. M. Jayabalakrishnan, M. Prasanthrajan, G. Balasubramanian, A. Lakshmanan, S. Selvakumar and J. E. John, *RSC Adv.*, 2023, **13**, 4757–4774.
67 A. O. Adeola, M. Cui and R. Naccache, *Environ. Technol. Innov.*, 2023, **32**, 103419.
68 M. Vakili, H. M. Zwain, A. Mojiri, W. Wang, F. Gholami, Z. Gholami, A. S. Giwa, B. Wang, G. Cagnetta and B. Salamatinia, *Water*, 2020, **12**, 2242.
69 J. Yu, C. Chi, B. Zhu, K. Qiao, X. Cai, Y. Cheng and S. Yan, *Sci. Total Environ.*, 2020, **700**, 134412.
70 X. Li, P. Li, W. Chen, J. Ren and W. Wu, *Materials*, 2023, **16**, 4260.
71 S. Jung, H. Yun, J. Kim, J. Kim, H. Yeo, I.-G. Choi and H. W. Kwak, *Int. J. Biol. Macromol.*, 2024, **257**, 128810.
72 W. Xu, W. Zhang, Y. Li and W. Li, *Korean J. Chem. Eng.*, 2016, **33**, 2659–2667.